Zinc promoted alumina catalysts for the fluorination of chlorofluorocarbons

Michael Jones, [1] Graham J. Hutchings,[1] David J. Willock,[1*] John Scott[2†] and Stuart H. Taylor[1*]

[1] Cardiff Catalysis Institute, School of Chemistry, Cardiff University, Main Building, Park Place, Cardiff, CF10 3AT, UK.

[2] Ineos KLEA, The Heath, Runcorn, Cheshire, UK.

* Corresponding authors: Email: taylorsh@cardiff.ac.uk Tel: +44 (0)29 20 87 4062

Email: willockdj@cardiff.ac.uk Tel: +44 (0)29 2087 4779

† Retired

Abstract

A range of catalysts consisting of zinc impregnated γ-Al_2O_3 has been examined for the fluorination of chlorofluorocarbons. Addition of zinc to γ-Al_2O_3 promotes steady state fluorination of $CF_2ClCFCl_2$ (CFC-113) to 1,1,1,2-tetrafluoro-2,2-dichloroethane (CFC-114a). Zinc promotion of fluorination activity was maximised at 6.5 wt%. Temperature programmed reaction (TPR) studies on pre-fluorided catalysts show that CCl_4 is fluorinated by a sequential mechanism, with CCl_3F a primary product and CCl_2F_2 a secondary product. The addition of zinc to γ-Al_2O_3 resulted in a low temperature feature in the TPR profile, and further analysis shows that there is a strong correlation between catalyst activity for CFC-113 fluorination and the concentration of fluorine associated with this low temperature feature. As the site population of the low temperature feature increases the apparent activation energy for the CFC-113 fluorination process decreases. Higher temperature HF pre-treatment resulted in a significant reduction of the population of this low temperature site compared to the standard conditions without pre-treatment, indicating that active fluorine consists of labile surface bonded H-F, rather than a metal fluoride such as AlF_3 or ZnF_2. Based on experiments investigating highly dispersed zinc on an activated carbon support, zinc adjacent to an Al^{3+} ion is required for fluorination, since this allows adsorption of active HF in close proximity to a Lewis acid site, where the CFC can adsorb.

Keywords: zinc, alumina, fluorination, chlorofluorocarbons, CFCs, TPR

1. Introduction

Chlorofluorocarbons (CFCs) and hydrochlorofluorocarbons (HCFCs) were developed for applications in refrigeration and air conditioning, where their thermodynamic properties coupled with low flammability make them ideal for use in heat exchangers. In the 1970s the link between atmospheric chlorofluorocarbons and the destruction of stratospheric ozone was established [1]. Subsequently, the magnitude of stratospheric ozone depletion was appreciated, leading to increased political pressure to restrict the use and emission of CFCs. As a consequence, in 1984, under the auspices of the United Nations, the Montreal protocol was agreed. This was the first international treaty relating to the protection of the environment. In 1987 the Montreal protocol finally gained commitment from governments around the world to reduce the production of CFCs to 50 % of the 1986 levels by 1999. This was followed by the London amendment in 1990, which agreed the complete phase out of CFC production in developed countries by 2000, and by 2010 in developing countries. In 2007 a further adjustment to these agreements accelerated the phasing out of HCFCs emitted to the atmosphere, with production and emission caps in 2013. Since 2013, monitoring has confirmed a stabilisation of the emission levels of HCFCs [2].

Against the background of environmental concerns, it became imperative to develop alternatives to CFCs with low ozone depletion potentials (ODP). Fluorine containing organic compounds emerged as the best candidates, combining the appropriate boiling points, low toxicity and non-flammability demanded by users in a wide variety of applications with zero ODPs. For example, 1,1,1,2-tetrafluoroethane (HFC-134a) is now used as a refrigerant, foaming agent and medical propellant. It has also been considered as a possible electrolyte material for a new generation of supercapacitors [3]. The wide spread availability of the

compound for these applications has also led to the investigation of HFC-134a as a chemical feedstock in pharmaceutical production [4].

Despite negligible ODP, HFC-134a has recently been banned in automobile air conditioning units, due to its high global warming potential (GWP = 1300). Consequently, the environmental impact of compounds such as HFC-134a are still a concern and emissions of HFCs in general are targeted for significant reduction moving forward from the 1998 Kyoto Protocol. A new generation of fluorinated olefins are now being developed to supersede the HFCs. One example is 2,3,3,3-tetrafluorpropene (HFO-1234yf) which has similar thermodynamic properties to HFC-134a and a zero ODP but also GWP of only 4 [5].

Both HFC and HFO compounds can be conveniently produced through the fluorination of CFCs with suitable catalysts. HFC-134a can be obtained by the successive fluorination of trichloroethene with HF over trivalent metal fluorides or oxides as catalysts [6]. Vapour phase catalytic fluorination using anhydrous hydrogen fluoride over fluorided catalysts is a widely adopted route for the industrial scale production of chlorofluoroalkanes, and is also a route to HFO compounds [7]. A number of studies have reported the use of fluorided chromia as a catalyst for the fluorination of CFCs. Work on the mechanistic aspects of this process have included radioisotope labelling experiments, which showed that ^{18}F from chromia pre-fluorided with $H^{18}F$ appears in the fluorinated products when the reaction is carried out at elevated temperatures (973 °C) [8]. Catalysts impregnated with zinc have also been found to be superior fluorination catalysts in comparison with their non-doped counterparts [9]. However, the use of chromia as an industrial material has disadvantages for the treatment and disposal of the waste catalysts.

In the present study the fluorination of chloro-alkanes over zinc supported on γ-Al_2O_3 has been investigated. Initial studies have examined the steady state fluorination activity for the fluorination of $CF_2ClCFCl_2$ (CFC-113). Whilst, in order to probe the catalytic reactivity the

reaction of CCl_4 on pre-fluorided Zn/γ-Al_2O_3 in the absence of gas phase HF was also examined using a temperature programmed reaction (TPR) approach. Even though conversion of CCl_4 is the simplest example of a fluorination reaction, the mechanism for this chlorocarbon fluorination has still not been precisely defined and our experiments were designed to identify key features of the catalyst required for activity. We also show that the low temperature activity for fluorination of CCl_4 is a good predictor for steady state fluorination of CFC-113, suggesting that our results give a general insight into the fluorination of CFC compounds to produce fluorinated alternatives.

2. Experimental

2.1. Catalyst preparation

A series of catalysts with varying zinc loadings, ranging from 0 to 12 wt.%, on γ-Al_2O_3 were prepared by wet impregnation using aqueous zinc chloride (12.58 g in 50 cm^3 deionised water). The required amount of zinc chloride solution was added to pre-weighed γ-Al_2O_3 (8-10 g, Harshaw Al-3996R, surface area = 200 m^2 g^{-1}). The mixture was stirred to ensure thorough wetting of the solid by the solution, heated on a hot plate to remove excess water and calcined in static air at 350 °C for 15 h. The resultant solid was pelleted and sieved, to a particle size of 0.5 – 1.4 mm.

Catalysts consisting of zinc supported on carbon (Zn/C (2 and 10 wt.%), and ZnO were also prepared. The Zn/C catalyst was prepared by impregnating Norit activated carbon (Norit-RBAA3, surface area = 2000 m^2 g^{-1}) with a solution of ZnF_2. The resulting material was mixed, dried and calcined using the same procedure described for the production of alumina supported catalysts. Zinc oxide (Aldrich, surface area = 5 m^2 g^{-1}) was used as supplied and was pelleted to a uniform particle size range of 0.5 – 1.4 mm before testing.

2.2. Catalyst characterisation

Catalysts were characterised by powder X-ray diffraction (XRD) using an Enraf Nonius PSD120 diffractometer with a monochromatic $CuK_{\alpha 1}$ source operated at 40 keV and 30 mA. Surface areas were determined by multi point N_2 adsorption at -196 °C, and data was treated in accordance with the BET method.

X-ray photoelectron spectroscopy (XPS) was carried out using a Surface Science Interface instrument with two X-ray sources. The first was a monochromatic aluminium source (M-Probe), and the second was a dual magnesium/aluminium non-monochromatic source. Catalyst samples were transferred into the spectrometer *via* a nitrogen-purged glove box. Samples were placed onto stubs using double-sided adhesive tape. Fine mesh iron grids were placed over the samples and an electron flood gun (0.5-1.0 eV) was used during analysis in order to improve compensation for charging. Analysis was largely carried out using the M-Probe source, operated at 10 kV and 12.5 mA, with a residual pressure in the analysis chamber of 5×10^{-9} torr. Binding energies were referenced with respect to adventitious carbon.

2.3. Catalyst testing

Micro-reactor apparatus: The reactor was constructed from nickel/copper alloy (Monel) and polytetrafluoroethene (PTFE) tubing. It was used to dry and fluorinate catalyst precursors *in situ*, as well as being used to examine catalysts under continuous flow conditions at atmospheric pressure. Further, it was also used to contain the catalyst during temperature programmed reaction studies. The catalytic reactor consisted of a 1/4-inch Monel U-tube, inside one end of which the catalyst was supported on a Monel gauze. A brass heat sink was clamped to the reactor tube around the catalyst. The heat sink jacket was fitted with thermocouples and

engineered to allow accurate controlled heating, and quick cooling via the incorporation of a liquid nitrogen gas-cooling unit. The reactor tube was situated within an oven, allowing accurate temperature control (± 2 °C). Further details of the experimental set up is included in Supplementary Data, Section S1 including schematics of the experimental equipment used (figures S1 and S2).

The reactants were delivered using saturators that were housed in an insulated thermostated bath with the temperature maintained by means of a liquid nitrogen chiller unit fitted with a temperature controller, ensuring that a high degree of thermal stability was maintained. Nitrogen flow rates through the saturators were controlled and monitored using thermal mass flow controllers.

Gas analysis was performed on-line using a Chrompak CP9000 gas chromatograph, fitted with a flame ionisation detector. The gas chromatograph contained a system of two Poraplot Q columns that were operated in series. These were separated by a 10-port valve, allowing isolation of the individual columns. This made it possible to analyse CCl_4 using the first column whilst CCl_3F and CCl_2F_2 were eluted from the second column. This system is well suited to short analysis times, allowing online injections to be taken at two-minute intervals. The apparatus was calibrated daily using a series of reactant and product standards.

Catalyst Fluorination: Prior to determining the steady state catalyst activity and temperature programmed reaction studies the catalyst sample (5 g) was pre-treated with HF. N_2 (100 cm^3 min^{-1}) was passed over the catalyst bed and the oven was heated to 300 °C for 30 min. This drying period served to remove water and weakly bound hydroxyl groups from the catalyst surface. Catalysts were exposed to HF/N_2 for 15 h at 300 °C. A consistent HF mass flow was established by passing N_2 through a thermostatically controlled Monel saturator containing HF, maintained at 5 °C ± 2 °C. The N_2 flow rate was set to approximately 5 cm^3 min^{-1} and then

adjusted to give an HF mass flow of 0.025 g min^{-1}, determined by the time required to neutralise known aliquots of a basic solution at the reactor exhaust. At the end of the 15 h period the HF flow was discontinued and nitrogen (100 cm^3 min^{-1}) was passed over the catalyst for a further hour at 300 °C. At the end of the fluorination procedure the fluorided catalyst was isolated, and stored in the reactor tube ready for use.

Steady State Activity: Steady state catalyst activity was measured by the fluorination of $CF_2ClCFCl_2$. The catalyst (0.5 g) was loaded into a 1/4-inch Monel reactor tube and conditioned in HF (120 cm^3 min^{-1}) and $CF_2ClCFCl_2$ (5 cm^3 min^{-1}) for 15 h at 300 °C. Both HF/N_2 (90 cm^3 min^{-1}) and $CF_2ClCFCl_2$ (10 cm^3 min^{-1}) flow rates were increased for determination of catalyst activity, which was performed at 300 °C. Samples were taken from the reactor exit line using a glass sample vessel (200 cm^3), sampling was carried out over a two minute period after which the glass vessel was closed via a two way tap. A syringe was used to withdraw 5 cm^3 of the gas which was injected into the gas chromatograph. The conversion of $CF_2ClCFCl_2$ was monitored as the total percentage of the fluorinated products. Sampling took place at 10 min intervals over a period of 1 h.

Temperature Programmed Reaction (TPR): Catalyst (0.5 g) was placed in the reactor tube, heated to 300 °C and dried for 30 min. Subsequently liquid nitrogen was used to cool the system to 50 °C. The catalyst was saturated with HF/N_2 (135 cm^3 min^{-1}) for 2 min followed by 15 min of purging with nitrogen. Liquid nitrogen was then used to cool the system to -35 °C, at which temperature the catalyst was conditioned over a period of 30 min with carbon tetrachloride (0.2 cm^3 min^{-1}). Then temperature programmed heating was commenced using a ramp rate of 2 °C min^{-1} and the carbon tetrachloride flow rate was increased to 2 cm^3 min^{-1} and analysis started. After 2 h the carbon tetrachloride flow rate was increased to 20 cm^3 min^{-1}. The predetermined

changes in the carbon tetrachloride flow rate were designed to prevent the catalyst surface becoming saturated at low temperatures and to avoid 100 % conversion of carbon tetrachloride at higher temperatures. The experiment was stopped when the reactor temperature reached 350 °C, and then the sample was allowed to cool under nitrogen (100 cm^3 min^{-1}). The reactor effluent was sampled throughout the experiment at 2 min intervals and analysed by gas chromatography.

3. Results

3.1. Catalyst characterisation

Table 1 summarises the BET surface areas of the series of Zn-doped γ-Al_2O_3 catalysts, measured in their pre- and post-fluorided states. For the pre-fluorided materials a higher zinc concentration appears to result in a lower catalyst surface area. However, a more significant decrease in surface area was evident when a catalyst was subjected to fluorination. For the lowest Zn loadings (0 – 0.25%) the surface area of the fluorided catalyst is lower than that of the equivalent material before fluorination by a factor of 6 or 7. An increased level of Zn appears to stabilise the pore structure of the alumina against fluorination, with the surface area of the highest loading materials (9 - 12% Zn/γ-Al_2O_3) having surface areas just over half of the pre-fluorided equivalents. This leads to a reversal in the trend of surface area with Zn loading, so that post-fluorination the highest loading of Zn gives a material with around twice the surface area of un-doped γ-Al_2O_3.

Figure 1 shows the X-ray diffraction patterns of γ-Al_2O_3 doped with increasing zinc concentrations. All of the patterns show characteristic γ-Al_2O_3 diffraction lines at 2θ = 67°, 46°, 39.5° and 37.5° [10]. Increasing the zinc content of the catalyst has the effect of decreasing the intensity of diffraction. Although the diffraction peaks can be assigned to a γ-Al_2O_3 defective

spinel-type structure, the low angle region shows broad peaks due to the inherent disorder of the structure. The peak broadening, and the decreasing intensity of the diffraction signal, suggest that there is a reduction of crystallinity upon the addition of zinc.

The diffraction patterns obtained for fluorided materials are shown in Figure 2. Diffraction peaks at $2\theta = 67°$ and 46° corresponding to γ-Al_2O_3 are still present for the fluorided alumina and Zn doped catalysts. However, these are broader than for the pre-fluorided materials and the lower angle peaks for the γ-Al_2O_3 phase are difficult to discern. For the undoped γ-Al_2O_3 material additional sharp diffraction peaks appear after fluorination, indicating the presence of AlF_2OH ($2\theta = 14.2°$, 30.8° and 32.1°) and β-AlF_3 ($2\theta = 15.8°$, 24.8° and 29.7°) [11]. This result is consistent with observations by DeCanio *et al.*, who previously explored the effect of different degrees of fluorination on the structure of γ-Al_2O_3 [10]. For fluorided zinc-impregnated alumina the peaks for these fluorided phases are less apparent, although the distinct peak at $2\theta = 24.8°$ may indicate that these materials contain a greater proportion of the β-AlF_3 phase than the fluorided γ-Al_2O_3 that has not been Zn doped. Comparing figures 1 and 2 we note that fluorination generally reduces diffraction intensities, especially for the higher zinc loadings, indicating a reduction in crystallinity on treatment of samples with HF.

X-ray photoelectron spectroscopy (XPS) was performed on 4% Zn/γ-Al_2O_3, 6.5% Zn/γ-Al_2O_3 and 10% Zn/γ-Al_2O_3 fluorided samples after use in the reactor studies. An example broad scan spectrum is given in figure S3 confirming that the fluorided samples contain Al, Zn, F and O in the near surface region. The surface atomic ratios for the used catalysts are shown in Table 2. The elemental surface concentrations were broadly similar for the different catalysts. Fluorine was the most abundant element demonstrating that a high degree of surface fluorination remains after the catalyst has been used. It is also apparent that a relatively high concentration of aluminium was also present on the surface of the catalysts. The aluminium concentration

increased as the zinc content was increased. Zinc was also observed to be present on the catalyst surface, but the concentrations were relatively low compared to the Zn doping levels present in these materials. It is interesting to note that a significant level of carbon was detected on all of the catalysts, however, residual chlorine and sodium was only present on the catalyst with 6.5% Zn.

High-resolution X-ray photoelectron spectra were also recorded, concentrating on the F 1s photoelectron peak, due to the high surface concentration of fluorine. An asymmetric peak shape was observed for the catalysts with different zinc loadings, which all showed broadly similar spectra. The asymmetric F 1s peak was resolved into two peaks by curve fitting and a summary of the data is presented in Table 3. The binding energies of both F 1s peaks decreased as the zinc loading was increased. It is difficult to give a definitive assignment of the fluorine species. The two species are most likely to be ZnF_2, 684.8 eV, and AlF_3, 686.3 eV, assigned against the values in the NIST Database. The shift of the binding energies from the values expected for ZnF_2 and AlF_3 species suggests that these may not be present as discrete species. Although the absolute binding energies of the F 1s peaks also shifted with zinc loading, the differences in binding energy between the two peaks did not change significantly. The differences in binding energies for the catalysts were 1.7 - 1.8 eV, and these values are very close to a difference of 1.5 eV obtained from the standard values in the database..The binding energy values for Zn $2p^{3/2}$ and Al 2p peaks are also given in Table S1 for the catalysts containing 4%, 6.5% and 10% Zn loadings. Comparing these values against standard references for Zn/Al containing oxides and fluorides (NIST, Table S2) shows that the fluorided catalysts have metal binding energies closer to the fluoride references than to the oxides (which occur at lower energies in each case). This observation indicates that there is a change of the metal environment on fluorination as fluorine anions are introduced into the materials and metal halide bonds replace metal oxide bonds..

3.2. Steady State Catalyst Activity

The steady state catalyst activity was established by measuring the rates of fluorination of $CF_2ClCFCl_2$ (CFC-113) in a continuous HF gas stream. Initially CCl_4 was used as the reactant but the fluorination reaction proved too facile, demonstrating high conversions even at low temperature. $CF_2ClCFCl_2$ was selected as the replacement, as the susceptibility to halogen exchange is related to the C-Cl bond strength. The C-Cl bond strength in $CF_2ClCFCl_2$ (326 kJ mol^{-1}) is higher than in CCl_4 (306 kJ mol^{-1}), and hence it is more resistant to fluorination [12]. The steady state rates of $CF_2ClCFCl_2$ fluorination over the range of zinc-impregnated catalysts are shown in Figure 3.

The reaction rates are presented as the mean of up to four separate repeat experiments, and they are shown as the percentage yields of CF_3CCl_2F (CFC-114a), the full data set is given in Table S3. The data clearly demonstrates the promotional effect of zinc addition to γ-Al_2O_3 by increasing conversion of $CF_2ClCFCl_2$ to CF_3CCl_2F. CF_3CClF_2 (CFC-115) and CF_3CF_3 (CFC-116) were also produced in the reaction, but these were only formed in trace amounts. Fluorination activity was a maximum with a zinc loading of 6.5 %. A further increase in the level of zinc impregnated on the alumina support caused a decrease in catalytic activity, although the surface area of this fluorided catalyst was generally higher for the higher loadings of Zn. No reaction was observed for fluorination of $CF_2ClCFCl_2$ over a fluorided alumina catalyst without zinc addition. Catalysts were tested for periods in excess of 120 h, and no significant deactivation was observed over this time period. Catalysts of zinc supported on activated carbon and ZnO were found to be inactive.

3.3. Temperature Programmed Reaction studies

As highlighted previously, steady state activity data for the zinc doped catalysts were determined for the fluorination of $CF_2ClCFCl_2$, as a consequence of the extremely high activity shown for CCl_4. However, fluorination of CCl_4 was investigated as a probe reaction in temperature programmed reaction studies. Figure 4 illustrates a typical temperature programmed reaction profile obtained by passing CCl_4 continuously over an HF pre-treated 0.5% Zn/γ-Al_2O_3 catalyst. After analysis for 2 h the CCl_4 flow rate was increased from 2 cm^3 min^{-1} to 20 cm^3 min^{-1} and this is manifested as a step around 150 °C in the TPR profile. The predetermined changes in the carbon tetrachloride flow rate were designed to prevent the catalyst surface becoming saturated with the chlorocarbon at low temperatures. Furthermore, above 150 °C the reaction rate was very high and a higher concentration of CCl_4 was required so that a conversion below 100 % was maintained. The TPR profile results show that the fluorinated reaction products were CCl_3F (CFC-11) and CCl_2F_2 (CFC-12); traces of $CClF_3$ were also present but these were always in negligible quantities. The total amount of fluorinated products ($CClF_3$ + CCl_2F_2) formed during the reaction is also plotted in the figure.

In the low temperature region (-35 °C – 150 °C) of the TPR plot shown in figure 4 CCl_3F (CFC-11) starts to appear at much lower temperatures than CCl_2F_2 (CFC-12). Conversion of CCl_4 to CCl_3F is apparent at even the lowest temperatures, and increases to a broad peak at around 18 °C with a second sharper peak at around 50 °C. Whereas the production of the difluoride, CCl_2F_2, only begins around 0 °C and has a single peak at 64 °C. This suggests that CCl_2F_2 is produced by the fluorination of CCl_3F rather than being formed as a primary product over this catalyst. In the high temperature range (150 °C – 350 °C) CCl_3F is the dominant product with the production of CCl_2F_2 dropping to zero for temperatures in excess of 240 °C. There are two clear peaks in the fluorination rate at around 190 °C and 275 °C. At these temperatures it is likely that bulk fluorine migration from the lattice to the surface occurs and the kinetics of this rate determining process, rather than that of the fluorination event, is being observed.

Similar TPR experiments were carried out for all of the catalysts, and in the remaining examples we simply show the low temperature region and the total rate of production of fluorinated products as this information relates directly to the fluorination event when CCl_4 reacts with the pre-fluorided surface.

Figure 5 shows the temperature programmed reaction profile for a γ-Al_2O_3 sample, which did not have zinc added. A single feature was observed at *ca.* 90 °C, and the line shape indicates that the fluorination of CCl_4 over pre-fluorided γ-Al_2O_3 is probably an autocatalytic process as the leading edge of the profile has a very steep gradient. There are none of the low temperature features that were noted for 0.5% Zn/Al_2O_3 (Figure 4).

Figure 6*a* and 6*b* show the low temperature regions of TPR profiles for fluorinated products (CCl_3F + CCl_2F_2) for example catalysts with Zn loadings of 0.1 % and 6.5 % respectively. The low temperature regions of such profiles for all loadings of Zn studied here were examined in detail to extract kinetic data from the initial low conversion regions. The data for the -35 – 25 °C region, in which site 1 is expected to be the dominant reaction centre was modelled by fitting a simple first order reaction scheme. Since the reagent CCl_4 is in large excess, the rate of reaction, *r*, can be assumed to be only dependant on the effective concentration of site 1, [*S*].

$$r = k_1[S] \qquad (1)$$

We also assume that the rate constant, k_1, depends on temperature, *T*, according to the Arrhenius equation, *i.e.*:

$$k_1 = Aexp\left(\frac{-E_a}{RT}\right) \qquad (2)$$

Where *A* and E_a are the pre-exponential factor and activation energy for individual sites of reaction, respectively. In order to use this model to represent the TPR profiles obtained experimentally we use a simple numerical integration scheme to obtain the remaining concentration of active sites as a function of time, *t*,

$$[S] = [S_0] - r\delta t = [S_0] - r\,\beta^{-1}\delta T \qquad (3)$$

Here δt is the time between integration points and we also note that the linear ramp rate, ($\beta = dT/dt = 2$ °C min^{-1}) used in this type of experiment allows integration with respect to time or temperature. It was found that the TPR curves in the fitting region are sufficiently smooth that integration with $\delta T = 0.5$ °C gave converged values of the parameters.

The fit to the observed rate was established by manipulation of the E_a and initial site population [S_0] parameters to provide a match to the experimentally determined fluorination rate profile using the least squares difference between the experimental and model curve in the low conversion regions. The fitted profiles are shown in Figures 6*a* and 6*b* and the fitted parameters are given in Table 4.

For the lowest loading of Zn (0.1%) figure 6*a* shows a peak at 75 °C, significantly lower than that observed for γ-Al_2O_3 alone (90 °C, Figure 5). Fluorination activity is also apparent from the start of the temperature ramp at -35 °C and the fitted function following equations 1-3 gives a peak at around 19 °C. This low temperature feature is assigned to activity due to a mixed Al/Zn site referred to here as site 1. Figure 6*b* shows the low temperature TPR region for the most active catalyst for the steady state fluorination of $CF_2ClCFCl_2$ (6.5% Zn/Al_2O_3) the proportion of the TPR curve accounted for by the fit to the site 1 activity is significantly greater than seen for the 0.1% Zn/Al_2O_3 sample. The fitted peak remains close to 20 °C and there is no additional peak observed in this temperature range.

The effect of increasing the zinc level in the catalysts on the fitted E_a and site 1 population, [S_0], is summarised in Table 4 and the site 1 population as a function of Zn loading is plotted in Figure 6*c*. Most catalyst compositions were tested at least four times through the preparation and testing of a new batch of catalyst for each TPR run. This allows determination of errors, given in Table 4 and the error bars shown in Figure 6*c*, to be estimated from the standard deviation of the sample to sample variation. It is apparent from Figure 6*c* that the site population

increases with Zn loading up to the 5% Zn/Al_2O_3. Above 5% zinc, within the error limits of our experiments, we conclude that the site 1 population is practically independent of Zn loading. The activity of 2% Zn/C, 10% Zn/C and ZnO were also investigated for CCl_4 fluorination by the TPR technique. All three materials were inactive for halogen exchange as no fluorinated products were observed in either the low or high temperature areas of the TPR profiles.

4. Discussion

4.1. Catalyst characterisation

In the present study definitive analysis of the zinc impregnated γ-Al_2O_3 by X-ray diffraction proved difficult due to the lack of long range ordered phases. γ-Al_2O_3, Has an intrinsically disordered structure which can be thought of as a defective spinel in which Al^{3+} occupied both octahedral and tetrahedral sites with partial site occupancy of the tetrahedral positions leading to disorder [13],[14]. When transition metals are added to alumina by impregnation it is possible that there is formation of either a surface spinel or that bulk phase metal oxides can be formed with phase separation [15]. Identification of surface spinel $ZnAl_2O_4$ phases by XRD is difficult as the lattice parameters of γ-Al_2O_3 and the spinel $ZnAl_2O_4$ are virtually identical. Even so, the observation of a decrease in crystallinity of γ-Al_2O_3, with the increasing addition of zinc, observed by examination of the XRD patterns presented in Figure 1, is not accompanied by the introduction of the additional features that would be expected for phase separation of ZnO. In earlier work, Strohmeier and Hercules [16] also examined the interaction of Zn^{2+} with γ-Al_2O_3 using XRD, and observed broad diffraction peaks for γ-Al_2O_3, indicating poor crystallinity. Catalysts with zinc loadings below 10 %, showed XRD patterns that were identical to the support and they concluded that at these low loadings zinc is probably too highly dispersed to

cause any noticeable change in the alumina structure. Strohmeier and Hercules also examined zinc loadings greater than 12 % and found an increase in the intensity of diffraction peaks related to a $ZnAl_2O_4$ spinel-like phase. Lo Jacono and Schiavello [15] have also reported that when zinc is supported on γ-Al_2O_3 the formation of a surface spinel or bulk like ZnO phase occurs, often concurrently.

El-Hakam [17] has also examined the ZnO/Al_2O_3 system using XRD and reported that the crystal structure was dependent on chemical composition and calcination temperature. For zinc oxide contents in the scope of our work, there was no evidence for formation of crystalline ZnO or $ZnAl_2O_4$ spinel phases, and it was suggested that γ-Al_2O_3 inhibits crystallisation of ZnO at coverages less than 30 % zinc. It must be noted that this work was carried out using catalyst calcination temperatures far in excess of those used in this study.

Our analysis of the XRD data for γ-Al_2O_3 following fluorination with HF, shown in figure 2, suggests the formation of a more crystalline structure consisting of metal fluoride (β-AlF_3) and metal oxyfluoride (AlF_2OH). However, no evidence of separate phases of fluorided zinc could be established by XRD. Figure 2 also shows XRD patterns for the fluorinated Zn/γ-Al_2O_3 materials in which the sharp features associated with β-AlF_3 are less apparent and decrease with Zn loading. This would suggest that, for the Zn impregnated catalysts at least, the fluorided material maintains a spinel like structure even after fluorination and that the conversion to an AlF_3 structure through fluorination of the material is incomplete.

For all catalysts XPS analysis demonstrated that, after fluorination using our standard conditions, the surface consists of more than 50 % fluorided species. Kemnitz *et al.* [18] have also considered the effect of fluorination on γ-Al_2O_3 using XPS. It was proposed that a charge transfer accompanied the exchange of OH^- with F^- on the surface from Al to F atoms. This mechanism results in an increase of the material's Lewis acidity, and hence exerts an important

controlling influence on catalytic activity. Strong Lewis acid sites have been identified for the surfaces of β-AlF_3 [19] and linked to surface Al^{3+} cations co-ordinated by five bridged F^- anions [20]. However, the thermodynamically stable α-AlF_3 phase has no exposed surfaces containing this species and correspondingly has a low Lewis acidity [19] and shows no activity for fluorination reactions [21].

Our XPS results also show that the surface concentration of zinc is relatively low compared to the percentage of Zn used in catalyst preparation. The interaction of Zn^{2+} with γ-Al_2O_3 has also been probed using XPS by Strohmeier and Hercules [16]. Using $ZnAl_2O_3$ and ZnO as reference compounds, they found that at zinc loadings below 20 % there is the formation of a zinc surface spinel, whereas at zinc loadings over 20 % a ZnO phase is formed. Surface spinel formation was explained by the strong tetrahedral (T_d) site preference of the Zn^{2+} ion and their diffusion into the vacant T_d sites of the γ-Al_2O_3 lattice. Once all the T_d lattice sites are saturated (20% Zn) further addition of zinc can only be accommodated by segregation of a separate ZnO phase. The relatively high carbon levels on the catalyst surface observed in our XPS data (Figure S3 for example) are most likely due to adsorbed CFC fragments formed during reaction. The carbon content could also be due to coking of the catalyst surface, however CHN analysis does not support the formation of appreciable coke as the carbon levels detected post-reaction were negligible.

In summary, the addition of zinc to the γ-Al_2O_3 support results in a high dispersion of the zinc on the surface. The zinc impregnated materials have XRD patterns very similar to γ-Al_2O_3 with no additional ZnO phase observed. This suggests that the main Zn species present is Zn^{2+} incorporated into the tetrahedral sites of the defective spinel structure of the host material. Strohmeier and Hercules [16] also observed that, at the levels of zinc used here, up to 12 % by weight, formation of a $ZnAl_2O_4$ 'spinel' like phase occurs, with ZnO formation and segregation

only occurring at much higher zinc loadings. On fluorination β-AlF_3 can be seen in the γ-Al_2O_3 samples but this is less evident for Zn impregnated catalysts. This conclusion is also supported by our XPS data on the fluoride catalyst samples containing 4-12% zinc.

4.2. Catalyst performance

Steady state catalyst activity data clearly demonstrate that there is an optimum loading of zinc for the fluorination of $CF_2ClCFCl_2$ (Figure 3) of around 6.5 % by weight. The temperature programmed reaction studies using CCl_4 as a probe were used to help understand the origin of fluorination activity in these catalysts. For CCl_4 we observed significant quantities of both CCl_3F and CCl_2F_2. The exchange of multiple fluorine atoms may proceed via either a sequential mechanism or in a single event at a site capable of exchanging multiple fluorine atoms simultaneously. Waugh *et al*. have reported TPR experiments in the range 30 – 1070 °C for the fluorination of CCl_3F over fluorided chromia catalysts and report signals associated with the production of both CCl_2F_2 and $CClF_3$ at 250 °C and at 950 °C [22]. This suggests that, on the chromia catalysts, mono and di-fluorinated products are simultaneously produced with $CClF_3$ being created at a single site where two F atoms can be simultaneously delivered from the surface. They estimated very similar activation energies for both mono and di-fluorination processes (53 and 54 kJ mol^{-1} respectively), and assigned the lower productivity of $CClF_3$ to a lower site density for the di-fluorination active site. However, Rowley *et al*. [8], Kemnitz [23] and Gambarreto *et al*. [24] have argued that the fluorination of CCl_4, over chromia and aluminium fluoride, follows a sequential route to the di-fluorinated product.

The operation of a sequential fluorination reaction pathway, *i.e.* $CCl_4 \rightarrow CCl_3F \rightarrow CCl_2F_2$, is supported by the low temperature region of our own TPR results (figure 4) as the mono and di-fluorinated products are seen at different temperatures to one another. The TPR profiles show fluorination at very low temperatures, with CCl_3F appearing from -35 °C and CCl_2F_2 from

around 0 °C. We do note that at temperatures above 160 °C we see much lower production of the di-fluorinated product (in our case CCl_2F_2) than the mono-fluorinated product and that in this regime the two products give peaks at similar temperatures in the TPR.

As highlighted previously, the site concentration, [S_0], of the low temperature site 1 identified in the temperature programmed reaction studies, appears to be important in determining catalyst activity for the fluorination of $CF_2ClCFCl_2$. The γ-Al_2O_3 catalyst, which did not contain zinc, was inactive under the conditions used to probe steady state $CF_2ClCFCl_2$ fluorination. The same catalyst showed a broadly similar TPR profile to active catalysts containing zinc at high temperatures (> 100 °C), but significant differences were observed between the profiles below 100 °C. Most notably the zinc-promoted catalysts showed a low temperature feature that was absent for γ-Al_2O_3 (compare Figures 5 and 6). The correlation between catalytic activity for steady state $CF_2ClCFCl_2$ fluorination at 300 °C and the site 1 population as measured by CCl_4 fluorination is presented in Figure 7. A clear linear relationship between activity and site 1 population can be seen. Figure 7 includes data from the full set of catalysts prepared for this study. This strongly suggests that the site 1 population, apparent in TPR profiles in the 15 – 20 °C temperature range, is associated with the active site involved in the fluorination of $CF_2ClCFCl_2$.

The site 1 population can be increased / decreased depending on the dose / purge conditions of HF over the catalyst prior to TPR analysis. Figure 8 illustrates the effect of the temperature at which the HF dose and purge over the catalyst was carried out on the calculated site 1 area. Changing the HF dose / purge temperature directly effects site 1 characteristics. The decrease in site 1 area as the HF dose temperature is increased suggests that site 1 is related to a fluorine source labile at relatively low temperature, < 100 °C. The surface fluorine atoms of zinc fluoride or aluminium fluoride would not be expected to be labile at these low temperatures. This effect

suggests that active surface fluorine is present in the form of weakly bound surface HF molecules. Such an HF species would be labile at the temperatures used in the study and would explain the reduction in site 1 population when the HF dose / purge temperature was increased. However, it is important to note that all the catalysts were pre-treated and tested using the same procedures, and the differences observed are therefore due to differences between the reactivity of catalysts.

The best resolution of the site 1 feature in the TPR studies was achieved by HF dosing at 50 °C. Use of lower temperatures led to masking of the site due to HF adsorption, whereas, at higher temperatures, the concentration of site 1 was significantly reduced. This is consistent with the suggestion that the feature is associated with a weakly bonded labile surface HF species, rather than an inorganic species, such as ZnF_2 or AlF_3, which would be significantly less labile. HF dosing of the zinc modified catalyst at 30 °C produced a TPR profile similar in shape to that of fluorided γ-Al_2O_3, but with the peak maximum at a lower temperature. The gradient of the TPR line shape of γ-Al_2O_3 suggests an autocatalytic process. Again this could be due to HF initially blocking the active site and then desorbing as the temperature increased to reveal the active sites for CCl_4 adsorption and so giving rise to a rapid increase in the fluorination rate. This agrees with the dosing conditions, which would saturate the catalyst surface with HF multilayers that would impede halocarbon access to the active surface.

Further evidence for the importance of the site 1 feature controlling catalytic activity can be observed in a plot of the apparent activation energy as a function of site population (Figure 9). As the site 1 population increases the apparent activation energy for the reaction decreased from 40 kJ mol^{-1} to 25 kJ mol^{-1}. The decrease of the activation energy suggests that addition of zinc to γ-Al_2O_3 is providing a more energetically favourable pathway for the fluorination of chlorocarbons.

In the high temperature regime (>150 °C) the TPR profiles were very similar for all of the catalysts investigated. Furthermore, examination of the features in the high temperature section of the TPR profiles showed no correlation with activity. In the temperature range 150–375 °C it is probable that fluorine from the fluorided catalyst lattice migrates to the surface to react with the chlorocarbon.

Bankhead *et al.* [25] have used periodic DFT calculations to study the halogen exchange mechanisms for a fluorided alumina surface. They suggest that surface Al^{3+} cations act as Lewis acid centres, where HF can adsorb and dissociate. The mechanism of F/Cl exchange, for the example of CH_2Cl_2 they use, then takes place with the chlorocarbon adsorbed to a neighbouring Lewis acid centre and surface fluorine adding in an S_N2 type transition state. The Cl^- leaving group in this mechanism is stabilised by the surface Al^{3+} to which the molecule was adsorbed. Following this mechanism it is possible that zinc doping of alumina improves activity through enhancement of the material's Lewis acidity. This would increase the CFC contact time with the catalyst *via* an increase in the strength of adsorption of the CFC on the catalyst surface, and provide further stabilisation of a Cl^- leaving group. The addition of zinc may also alter the surface structure of γ-Al_2O_3, and we have noted that the surface area of our fluoride materials increases with Zn loading (Table 1). We also note that calculations on the CCl_2F_2 dismutation reaction over β-AlF_3 give a similar picture; with adsorption of the reactant at an Al^{3+} centre on the surface followed by halogen exchange with lattice F^- [20]. The common factor for these two models is the requirement of surface Lewis acid sites at which adsorption of the reagents can take place. As discussed, our XRD analysis suggests that the addition of Zn to γ-Al_2O_3 leads to a material that largely maintains the spinel lattice of the γ-Al_2O_3 even after fluorination. In contrast, for γ-Al_2O_3 without Zn incorporation we see clear β-AlF_3 peaks appear after HF treatment. However, this material has a much lower activity than the Zn impregnated catalysts

and so in discussing the structure of the active phase we will concentrate on the idea of a $Zn/\gamma\text{-}Al_2O_3$ spinel structure.

The geometry of the surface of fluorided zinc impregnated $\gamma\text{-}Al_2O_3$ is complex. Chen and Zhang. [26] have examined the exposed crystal planes of $\gamma\text{-}Al_2O_3$ using neutron diffraction studies of adsorbed CD_4, proposing that on the surface of $\gamma\text{-}Al_2O_3$ the (110) plane is preferentially exposed. A representation of the fluorided (110) plane of $\gamma\text{-}Al_2O_3$ is illustrated in figure 10. Catalyst characterisation has shown that fluorination of $\gamma\text{-}Al_2O_3$ results in fluorination of surface species and into the bulk structure whilst retaining the defect spinel structure. In the representation of fluorided $\gamma\text{-}Al_2O_3$, Al^{3+} cations occupy all the tetrahedral and octahedral positions available. Mardilovich [27] suggests that it is likely that there are cation vacancies in predominantly tetrahedral locations on the surface of $\gamma\text{-}Al_2O_3$. Addition of Zn^{2+} cations could fill these vacancies. In figure 10B) a model for the surface geometry of fluorided $Zn/\gamma\text{-}Al_2O_3$ (110) plane is proposed. Zn^{2+} cations are located in tetrahedral cation positions in the fluorided $\gamma\text{-}Al_2O_3$ structure adjacent to octahedral Al^{3+} cations. It is suggested that Zn^{2+} ions preferentially occupy the tetrahedral (T_d) sites due to their greater ionic radius. This argument is supported by Strohmeier *et al.* [16] who propose that Zn^{2+} ions occupy tetrahedral (T_d) sites on $\gamma\text{-}Al_2O_3$. Although not shown in the figure, it is likely that some Zn^{2+} cations may also be located in octahedral sites.

In the present study the addition of zinc to $\gamma\text{-}Al_2O_3$ is critical to activate the catalyst with respect to fluorination. It is proposed that the mechanism of fluorination and fluorination activity over zinc on $\gamma\text{-}Al_2O_3$ relies on the ability of zinc to provide a source of active HF species, enabling fluorine exchange with the adsorbed chlorocarbon. The relationship between surface zinc and HF to induce fluorine exchange could be ZnF–H–F, where the terminal F is involved in the substitution reaction with chlorocarbon. A similar mechanism has been suggested by Brunet *et*

al. [28], although the terminal fluorine atom is present as the last fluorine atom at the end of an HF oligomer chain. The absence of activity observed towards $CF_2ClCFCl_2$ fluorination over fluorided γ-Al_2O_3 may, then, be due to the lack of the Lewis acid centres, required for an active site where labile HF and/or the $CF_2ClCFCl_2$ can adsorb. Zinc on the surface of fluorided γ-Al_2O_3 seems to limit the production of the β-AlF_3 phase and leaves available Lewis acid centres. Although Zn^{2+} would have Lewis acidity in its own right, it is suggested that $CF_2ClCFCl_2$ adsorbs preferentially to the stronger Al^{3+} Lewis acid centre [29].

As previously suggested, surface zinc atoms on γ-Al_2O_3 could act as Lewis acid sites for HF adsorption, and chlorocarbon adsorption and activation. However, our results also suggest that a combination of aluminium and zinc sites must be present to obtain an active fluorination catalyst. Studying both fluorided ZnO and fluorided zinc supported on high surface area activated carbon, which was expected to reproduce zinc in a highly dispersed form showed these materials were inactive for fluorination catalysis. These results infer that zinc fluoride or a zinc oxy fluoride species was not singularly responsible for the fluorination activity of Zn/γ-Al_2O_3, adding further support for the proposal that an aluminium based active centre, such as an Al^{3+} Lewis acid site is required alongside Zn^{2+} to catalyse the fluorination process. The requirement for both aluminium and zinc sites present together would help to explain the *volcano* type plot for steady state fluorination activity (Figure 3).

From the current literature details of the mechanism for Cl/F exchange are not clear. Kemnitz *et al.* [30] have attempted to differentiate between the Langmuir-Hinselwood and Eley-Rideal mechanisms using the gas phase fluorination of CCl_4 over chromia catalysts. It was proposed that a Langmuir-Hinselwood mechanism occurred during fluorination, with reactants adsorbing at different sites on the catalyst. This was also supported by Coulson [31], who also suggested a Langmuir-Hinshelwood mechanism for the fluorination of $CHClFCF_3$ over HF pre-treated 2

% $CoCl_2$ on Al_2O_3. Modification of γ-Al_2O_3 with zinc increases the rate of fluorination and it is proposed that this is due to an energetically more favourable route for the delivery of HF to the chlorocarbon. It is interesting to note that for the Langmuir- Hinshelwood mechanism the rates of surface diffusion will also be important and it has been suggested that zinc also provides a lower energy route for fluorine migration across the surface to the active sites [9].

5. Conclusions.

Addition of zinc to γ-Al_2O_3 induces and promotes steady state fluorination activity of $CF_2ClCFCl_2$ (CFC-113). Zinc promotion of fluorination activity continues to increase up to 6.5 % zinc loading; further addition of zinc to γ-Al_2O_3 causes a reduction of catalyst activity. Temperature programmed reaction studies have been shown to be valuable for probing the fluorination activity, and show that CCl_4 is fluorinated by a sequential mechanism, with CCl_3F as a primary product and CCl_2F_2 a secondary product. The addition of zinc resulted in a low temperature feature in the TPR profile. Analysis of the low temperature feature shows that there is a strong correlation between catalyst activity and the concentration of fluorine associated with this low temperature feature on the catalyst surface. As the site population increased the apparent activation energy for the fluorination process was reduced. Higher temperature HF pre-treatment, compared to the standard conditions, resulted in a large reduction of the low temperature site population, indicating that active fluorine consists of labile surface bonded H-F rather than an inorganic species such as ZnF_2.

It is suggested that the surface of the catalyst undergoes fluorination to multilayer depth whilst retaining its defect spinel structure. Zn^{2+} cations preferentially occupy tetrahedral vacancies that exist on the catalyst surface adjacent to octahedrally located Al^{3+} cations. Addition of zinc to γ-Al_2O_3 activates the catalyst in respect of the fluorination of $CF_2ClCFCl_2$ by allowing adsorption

of active HF adjacent to an Al^{3+} Lewis acid site, which adsorbs the CFC. It is proposed that the relationship between surface Zn and HF to induce fluorine exchange involves the formation of a species like ZnF–H–F, where the terminal fluorine atom is involved in the substitution reaction with the halocarbon. Thus, Zn and Al cations need to be present on the surface simultaneously; Zinc is required to provide a labile surface fluorine species enabling reaction with adsorbed CCl_4. The CCl_4 is adsorbed to an Al^{3+} Lewis centre. The substitution reaction that occurs between the adsorbed molecules fluorinates CCl_4 to CCl_3F. HCl is also produced regenerating the Al^{3+} Lewis centre ready for adsorption by another CCl_4 molecule.

Acknowledgements

The Cardiff authors would like to thank Ineos KLEA for financial support.

Table 1. Measured BET surface of catalysts with various zinc content before and after fluorination.

Zn Wt.%	Surface Area, pre-fluornination / $m^2 g^{-1}$	Surface Area, post-fluorination / $m^2 g^{-1}$
0.0	206	28
0.10	168	24
0.125	168	28
0.25	202	32
0.50	181	39
0.75	146	36
1.0	191	64
1.5	162	50
2.0	174	43
3.0	154	46
4.0	168	42
5.0	167	53
6.5	151	45
9.0	132	76
10.0	118	63
12.0	109	58

Table 2. Atomic % of individual elements on the catalyst surface measured by XPS.

Element	Surface composition /at. %		
	4% Zn/ γ-Al_2O_3	**6.5% Zn/ γ-Al_2O_3**	**10% Zn/ γ-Al_2O_3**
Zn	0.79	1.52	1.31
F	61.91	54.61	58.04
Al	17.40	20.14	21.83
O	3.40	4.53	5.95
C	12.25	16.94	12.09
Na	0	0.31	0
Cl	0	0.79	0
N	1.16	1.15	0.79

Table 3. Binding energies and relative concentrations of fluorine species on the used catalyst surface determined by XPS.

Catalyst	Peak 2		Peak 2	
	Binding energy /eV	**Area /at. %**	**Binding energy /eV**	**Area /at. %**
4% Zn/ γ-Al_2O_3	685.6	15	687.2	85
6.5% Zn/ γ-Al_2O_3	685.3	8	687.1	92
10% Zn/ γ-Al_2O_3	685.1	19	686.9	81

Table 4. The effect of zinc loading on site 1 population and apparent activation energy for fluorination of CCl_4. Errors are estimated from standard deviations from 2-5 repeats of experiments where available.

Zn Level / % w/w	Site Population / mmol g^{-1}	Apparent Activation Energy / kJ mol^{-1}
0.100	0.026 ± 0.005	36.0 ± 0.7
0.125	0.027	41.8
0.130	0.033	39.7
0.250	0.064 ± 0.015	38.4 ± 1.2
0.500	0.046 ± 0.004	35.2 ± 0.6
0.800	0.094 ± 0.004	36.0 ± 1.3
1.000	0.079 ± 0.004	37.2 ± 1.1
1.500	0.090	35.6
2.000	0.077 ± 0.019	31.4 ± 2.2
3.000	0.169 ± 0.006	29.0 ± 0.5
4.000	0.139 ± 0.067	28.0 ± 1.5
5.000	0.241 ± 0.036	23.3 ± 1.7
6.500	0.168 ± 0.032	24.1 ± 1.5
8.000	0.235 ± 0.007	25.3 ± 0.3
10.000	0.169	25.1

Captions for figures

Figure 1. Powder X-ray diffraction profiles of zinc impregnated alumina catalysts.

Figure 2. Powder X-ray diffraction profiles of a series of fluorided zinc impregnated alumina catalysts.

Figure 3. Steady state rates of $CF_2ClCFCl_2$ fluorination as a function of zinc loading for Zn/γ-Al_2O_3 catalysts. Error bars are estimated from standard deviations from 2-5 repeats of experiments where available.

Figure 4. Temperature programmed reaction for the conversion of CCl_4 to CFC-11 ($CFCl_3$, red squares), CFC-12 (CF_2Cl_2, yellow diamonds) and total reaction rate (blue triangles). Catalyst: 0.5% Zn/γ-Al_2O_3 pre-dosed with HF (2 mins) and purged (100 cm^3 min^{-1} N_2, 15 mins). Reaction conditions: Temperature ramp rate β = 2 °C min^{-1}, flow rate N_2 to CTC saturator = 2 cm^3 min^{-1} up to 150 °C and 20 cm^3 min^{-1} thereafter. In separate experiments catalyst showed CFC113 conversion at 300 °C = 0.83 %.

Figure 5. Temperature programmed reaction of CCl_4 over HF pre-treated γ-Al_2O_3.

Figure 6. Temperature programmed reaction of CCl_4 over HF pretreated catalysts: *a*) 0.1% Zn/γ-Al_2O_3, *b*) 6.5% Zn/γ-Al_2O_3 and *c*) fitted site 1 population [S_0] as a function of percentage Zn loading of Zn/γ-Al_2O_3 catalysts. Error bars are estimated from standard deviations from 2-5 repeats of experiments where available.

Figure 7. Relationship between site 1 population from TPR studies for fluorination of CCl_4 using pre-fluorided catalysts and the steady state catalyst activity for fluorination of $CF_2ClCFCl_2$.

Figure 8. Temperature programmed reaction of CCl_4 over HF pre-treated 6.5% Zn/γ-Al_2O_3 using different HF doping temperatures prior to TPR analysis. HF doping temperatures are indicated on the right-hand side of each trace.

Figure 9. Relationship between apparent activation energy and site 1 population for the range of catalysts studied.

Figure 10. Representation of (A) fluorided (110) plane of γ-Al_2O_3. (B) Proposed fluorided (110) plane of Zn/γ-Al_2O_3.

Figure 1.

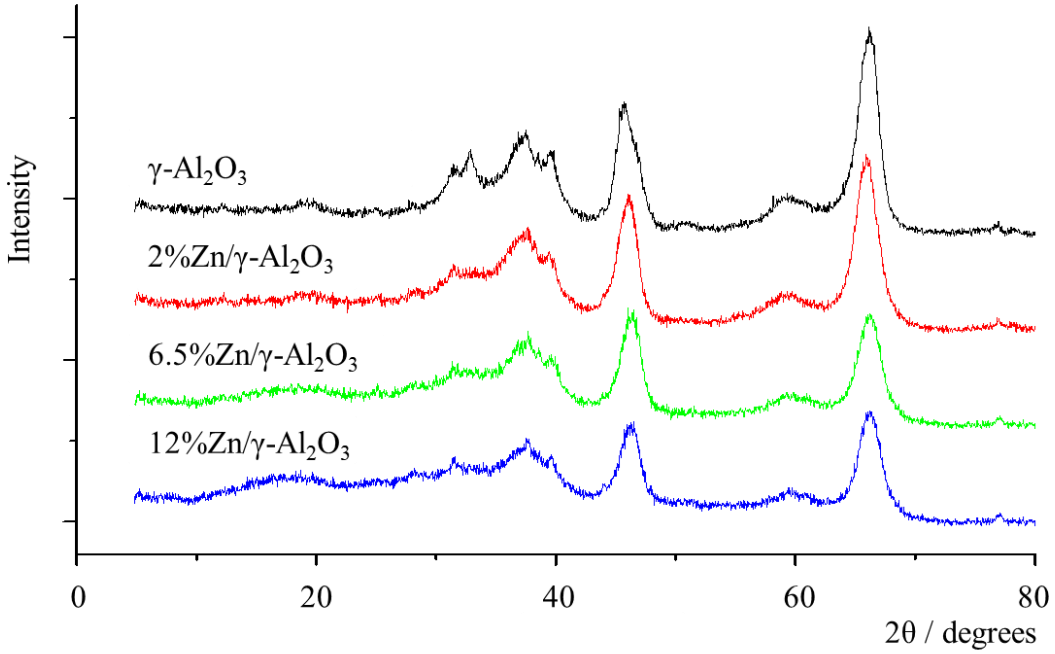
Intensity
γ-Al2O3
2%Zn/γ-Al2O3
6.5%Zn/γ-Al2O3
12%Zn/γ-Al2O3
0
20
40
60
80
2θ / degrees

Figure 2.

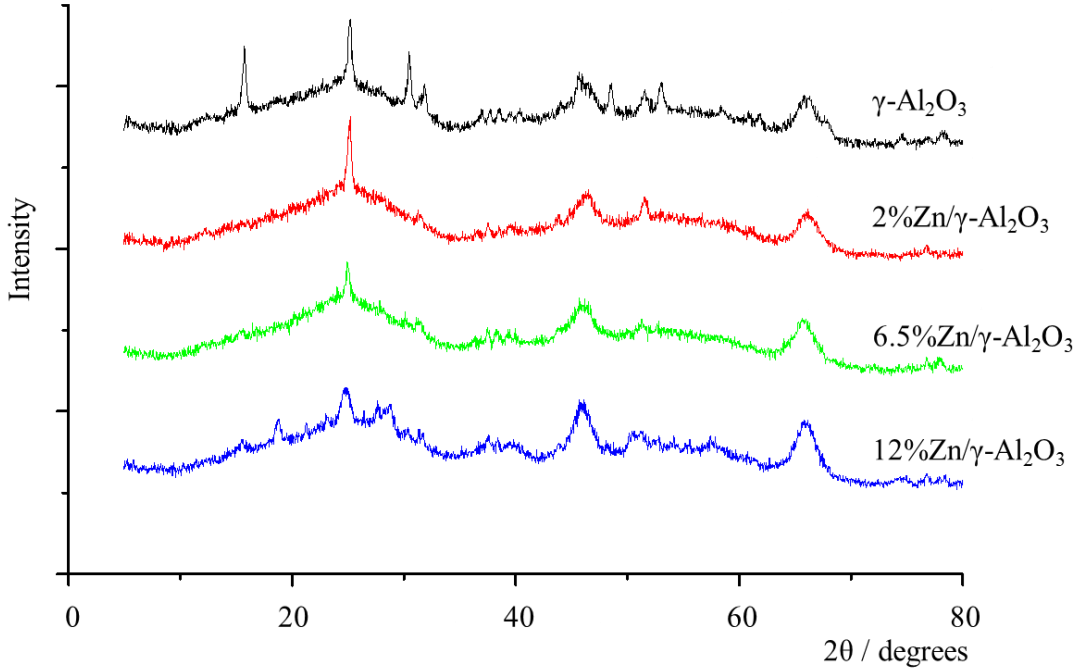
γ-Al2O3
2%Zn/γ-Al2O3
6.5%Zn/γ-Al2O3
12%Zn/γ-Al2O3
Intensity
0
20
40
60
80
2θ / degrees

Figure 3.

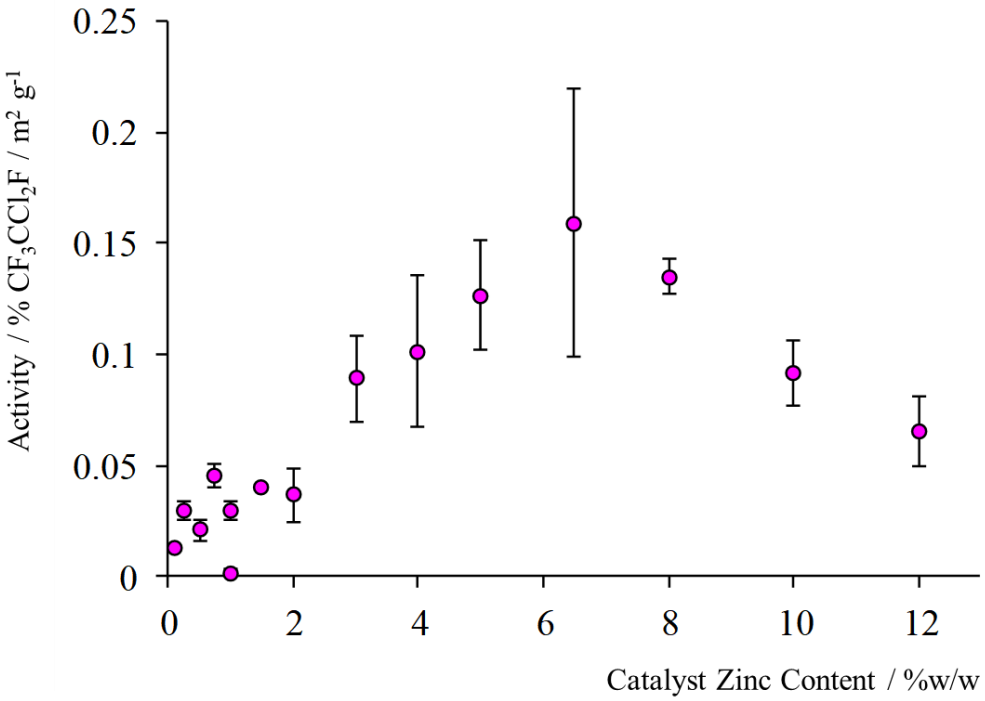
0.25
0.2
0.15
0.1
0.05
0
0
2
4
6
8
10
12
Activity / % CF_3CCl_2F / m^2 g^{-1}
Catalyst Zinc Content / %w/w

Figure 4.

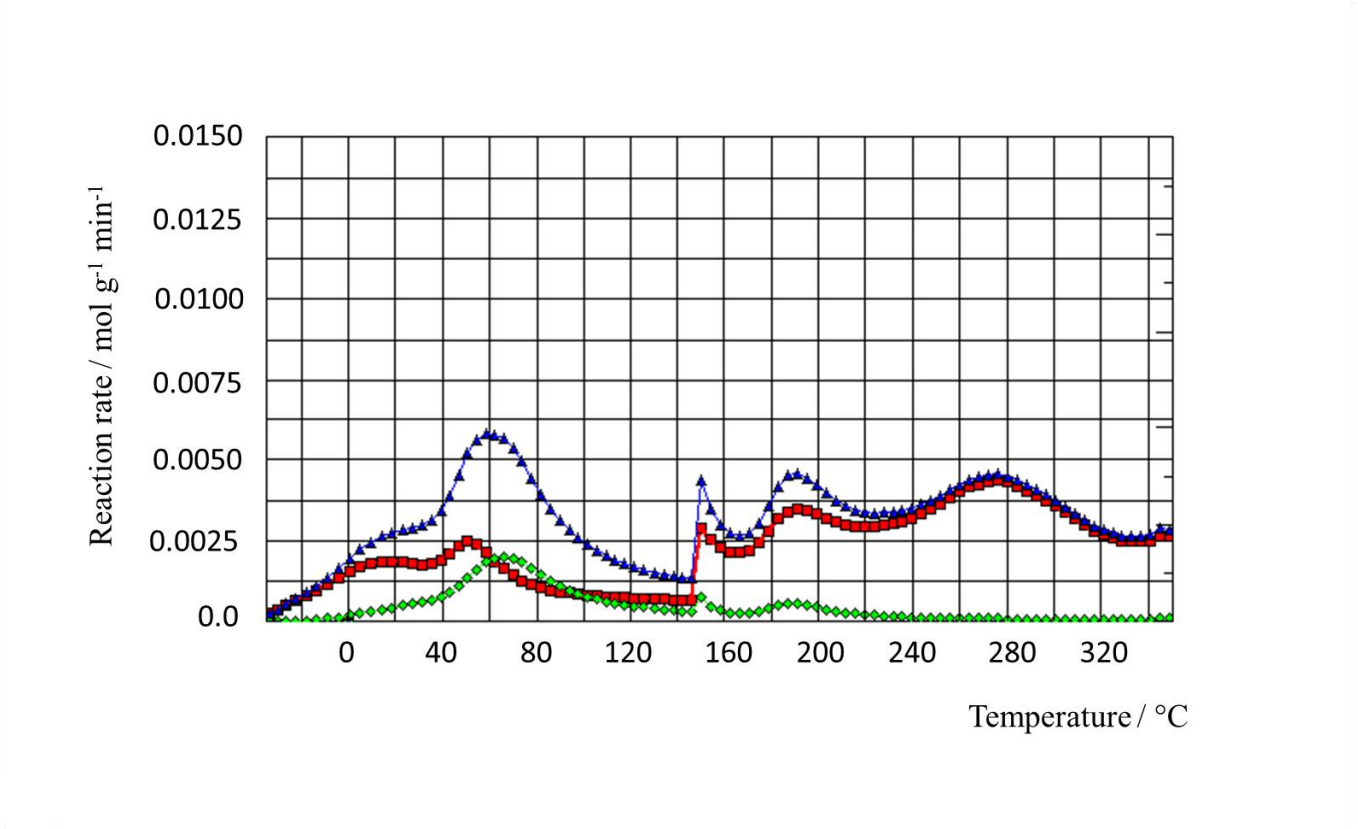
0.0150
0.0125
0.0100
0.0075
0.0050
0.0025
0.0
Reaction rate / mol g-1 min-1
0
40
80
120
160
200
240
280
320
Temperature / °C

Figure 5.

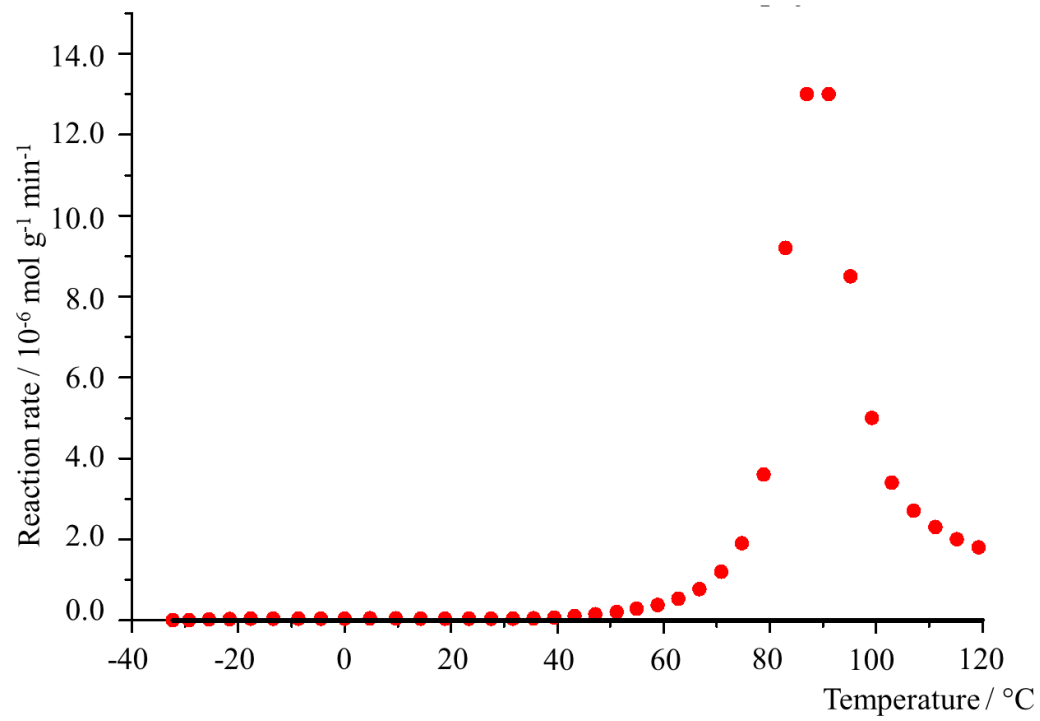
14.0
12.0
10.0
8.0
6.0
4.0
2.0
0.0
Reaction rate / 10-6 mol g-1 min-1
-40
-20
0
20
40
60
80
100
120
Temperature / °C

Figure 6.

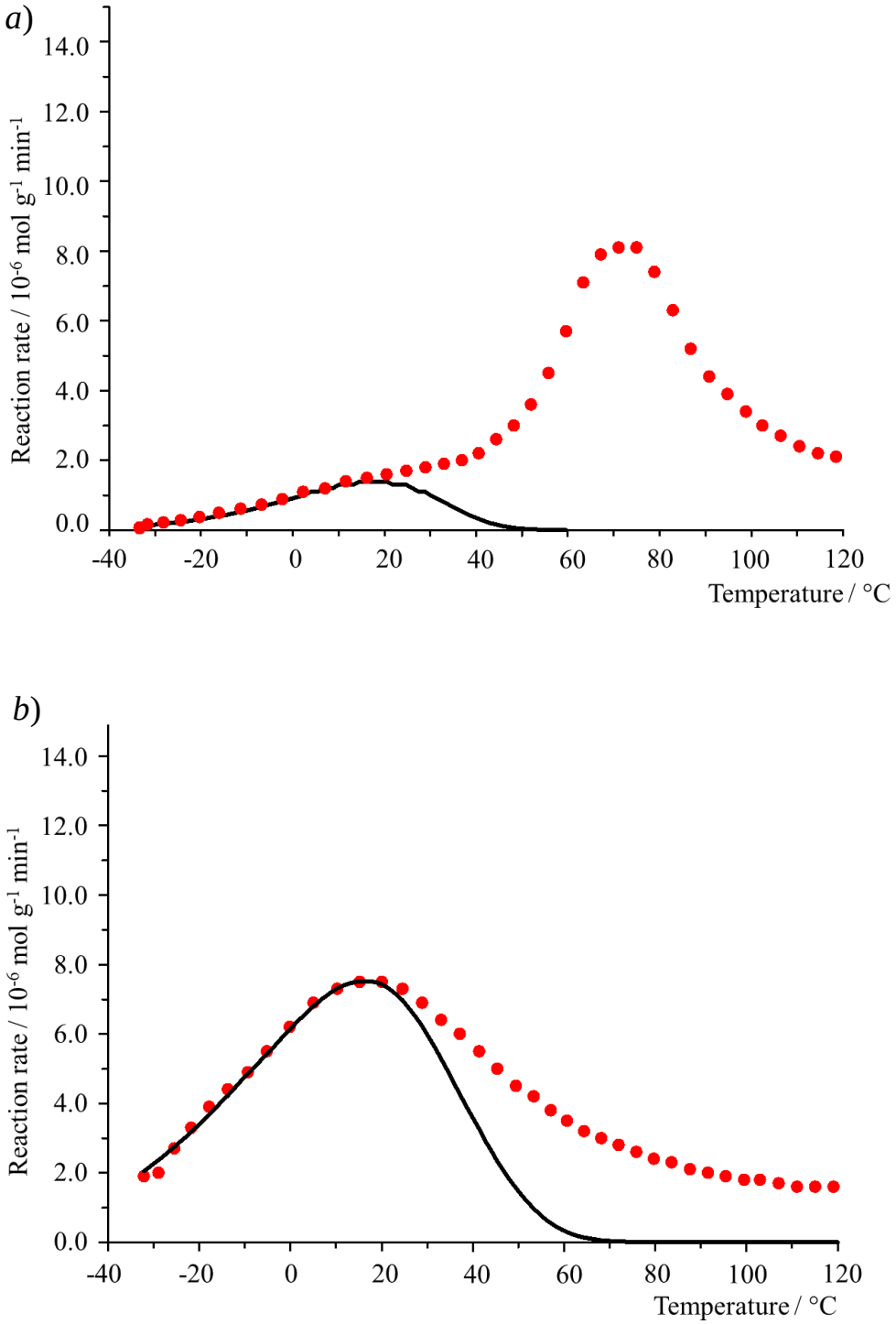
a)
Reaction rate / 10-6 mol g-1 min-1
14.0
12.0
10.0
8.0
6.0
4.0
2.0
0.0
-40
-20
0
20
40
60
80
100
120
Temperature / °C
b)
Reaction rate / 10-6 mol g-1 min-1
14.0
12.0
10.0
8.0
6.0
4.0
2.0
0.0
-40
-20
0
20
40
60
80
100
120
Temperature / °C

c)

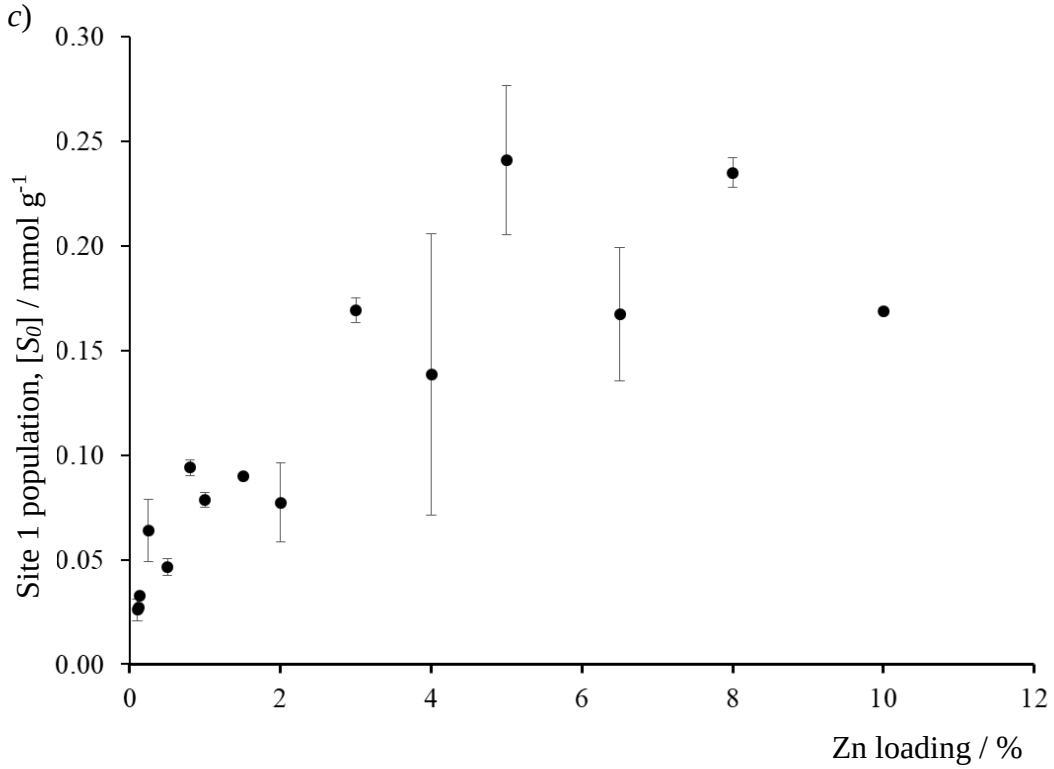
0.30
0.25
0.20
0.15
0.10
0.05
0.00
Site 1 population, [S0] / mmol g-1
0
2
4
6
8
10
12
Zn loading / %

Figure 7.

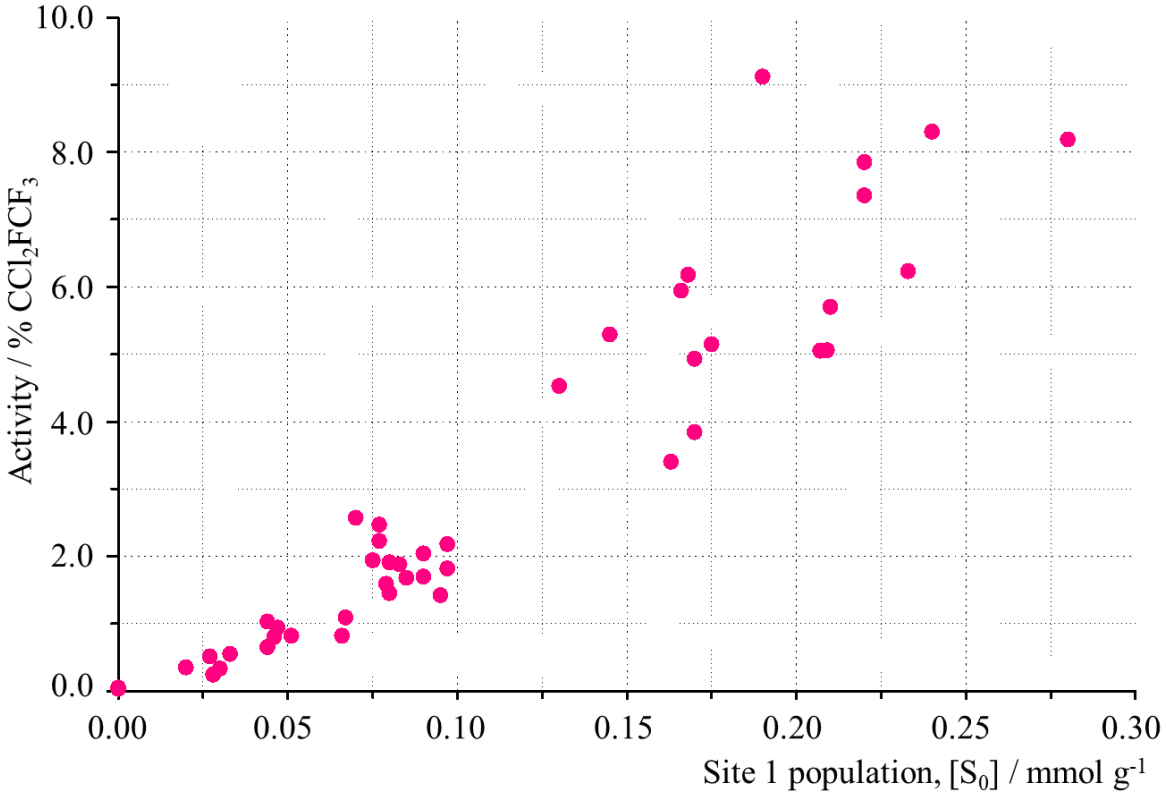
10.0
8.0
6.0
4.0
2.0
0.0
Activity / % CCl_2FCF_3
0.00
0.05
0.10
0.15
0.20
0.25
0.30
Site 1 population, $[S_0]$ / mmol g^{-1}

Figure 8.

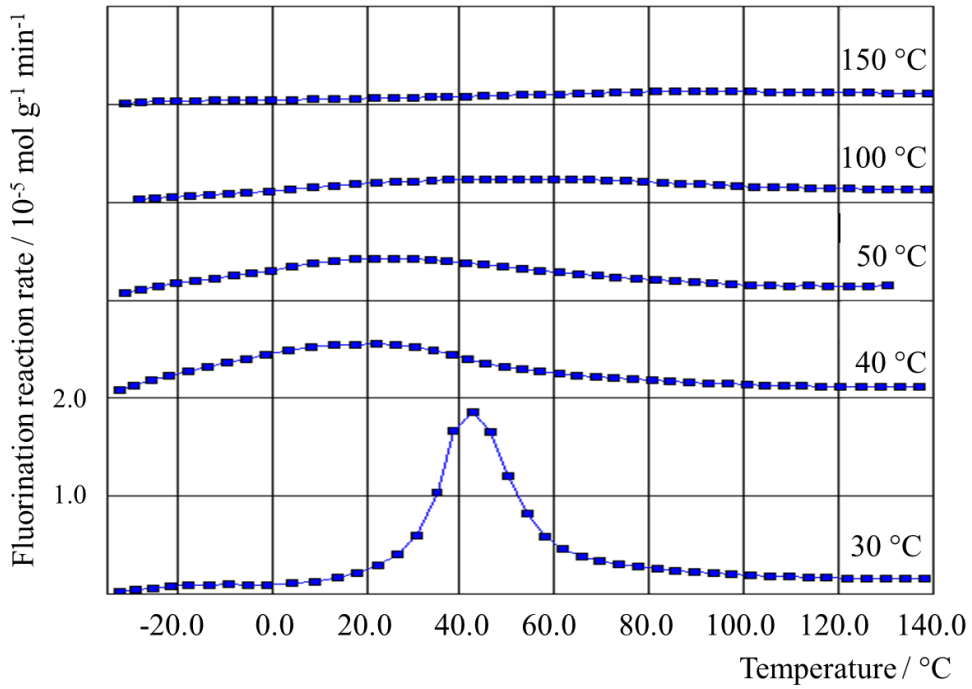
Fluorination reaction rate / 10-5 mol g-1 min-1
150 °C
100 °C
50 °C
40 °C
30 °C
2.0
1.0
-20.0
0.0
20.0
40.0
60.0
80.0
100.0
120.0
140.0
Temperature / °C

Figure 9.

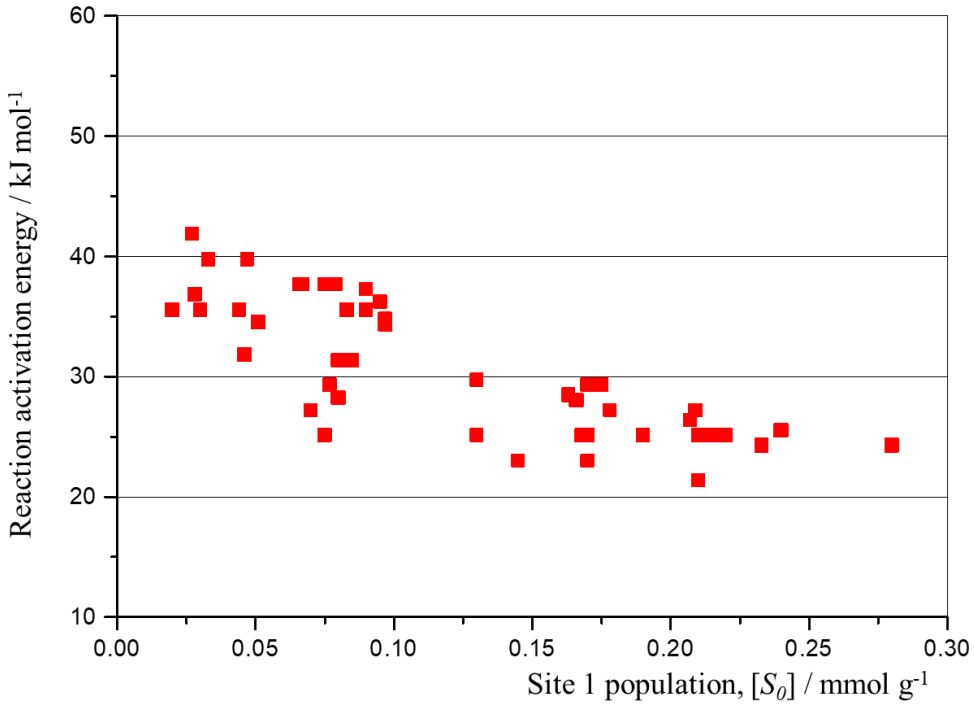
Reaction activation energy / kJ mol-1
60
50
40
30
20
10
0.00
0.05
0.10
0.15
0.20
0.25
0.30
Site 1 population, [S0] / mmol g-1

Figure 10.

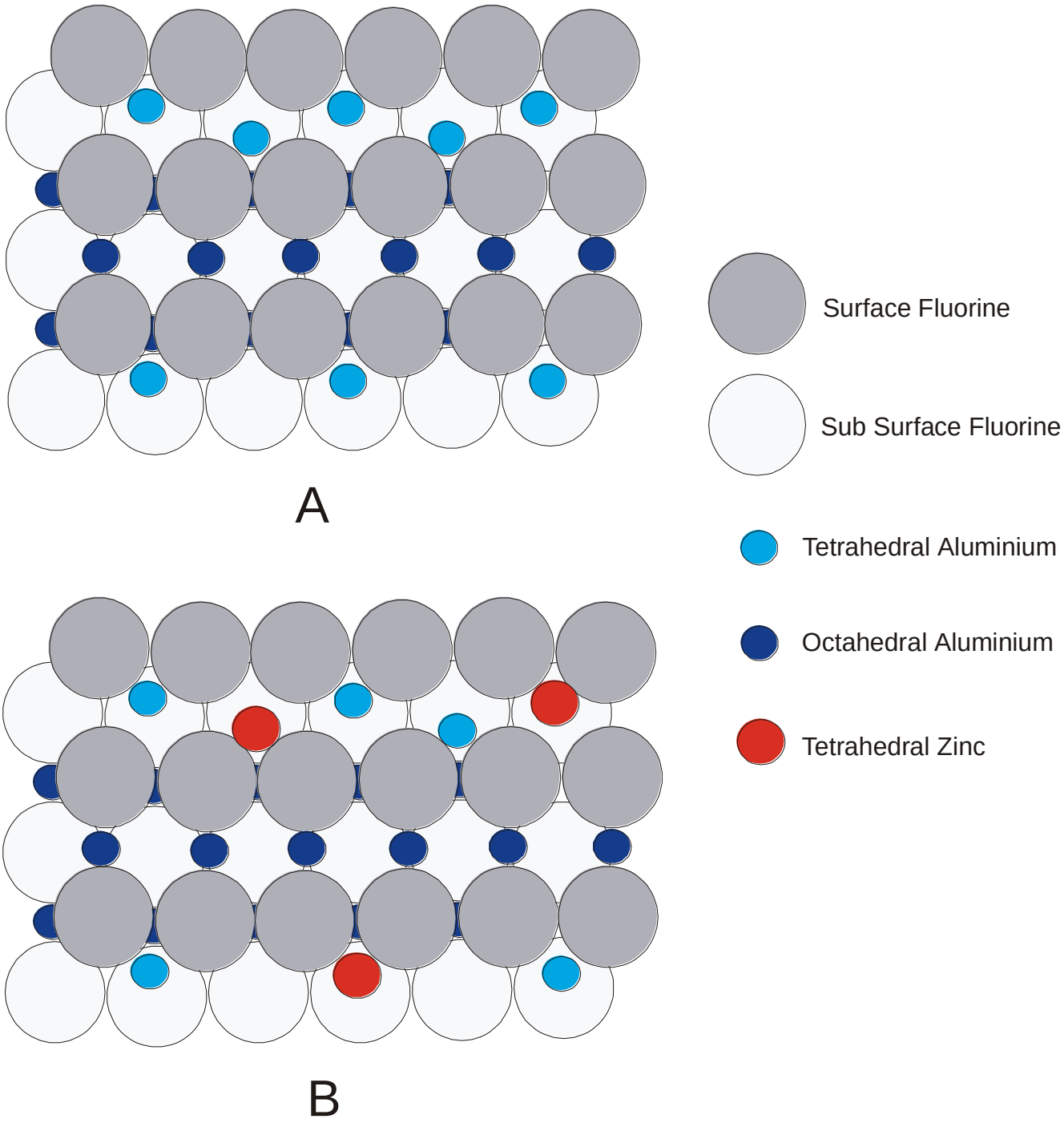
Surface Fluorine
Sub Surface Fluorine
Tetrahedral Aluminium
Octahedral Aluminium
Tetrahedral Zinc
A
B

References

1. M. J. Molina and F. S. Rowland, *Nature* **249**, 810-812, (1974).
2. P. G. Simmonds, M. Rigby, A. McCulloch, S. O'Doherty, D. Young, J. Mühle, P. B. Krummel, P. Steele, P. J. Fraser, A. J. Manning, R. F. Weiss, P. K. Salameh, C. M. Harth, R. H. J. Wang, and R. G. Prinn, *Atmos. Chem. Phys.*, **17**, 4641–4655, (2017).
3. C. S. Rustomji, Y. Yang, T. K. Kim, J. Mac, Y. J. Kim, E. Caldwell, H. Chung, Y. S. Meng, *Science*, **356**, 1351, (2017).
4. P.L. Coe, J. Burdon, and I.B. Haslock, *J. Fluor. Chem.*, **102**, 43-50, (2000)
5. S. Papasavva, D.J. Luecken, R.L. Waterland, K.N. Taddonio, S.O. Andersen, *Environ. Sci. Technol.*, **44**, 343–348, (2010).
6. A. Kohne and E. Kemnitz, *J. Fluor. Chem.*, **75**, 103-110, (1995), D. R. Corbin and V. N. M. Rao, U.S. Patent, 2000, 6,040,486.
7. W. Mao, L. Kou, B. Wang, Y. B. Bai, W. Wang and J. Lu, *Appl. Catal. A*, **491**, 37-44, (2015).
8. L. Rowley, J. Thomson, G. Webb J. M. Winfield and A. McCulloch, *Appl. Catal. A*, **79**, 89-103, (1991).
9. D. W. Bonniface, J. R. Fryer, P. Landon, J. D. Scott, W. D. Scott, M. J. Watson, G. Webb and J. M. Winfield, *Green Chem*. **1**, 9-11, (1999).
10. E. C. DeCanio, J. W. Bruno, V. P. Nero and J. C. Edwards, *J. Catal*, **140**, 84-102, (1993).
11. R. König, G. Scholz, K. Scheurell, D. Heidemann, I. Buchem, W.E.S. Unger and E. Kemnitz, *J. Fluor. Chem*., **131**, 91-97, (2010).
12. R. C. West., Ed. *Handbook of Chemistry and Physics*, 67th ed.; CRC Press: Boca Raton, Fl, (1987).
13. R-S. Zhou and R.L. Snyder, *Acta Cryst.*, B47, 617-630, (1991).
14. G.W. Watson and D.J. Willock, *Chem. Commun.*, 1076-1077, (2001).
15. M. Lo Jacono, M. Schiavello, *Preparation of Catalysts*, Elsevier, Amsterdam, (1976).
16. B. Strohmeier, D. M. Hercules, *J. Catal.*, **86**, 266-279, (1984).
17. S. A. El-Hakam, *Colloids and Surfaces A :Physiochem. Eng. Aspects*., **157**, 157-166, (1999).
18. A.Hess, E. Kemnitz, A. Lippitz, *J. Catal*, **148**, 270-280, (1994).
19. A. Hess and E. Kemnitz, A. Lippitz, *J. Catal*, **149**, 449-457, (1994).
20. C. L. Bailey, S. Mukhopadhyay, A. Wander, B. G. Searle, J. M. Carr and N. M. Harrison, *PCCP*, **12**, 6124-6134, (2010).
21. P.J. Chupas, M.F. Ciraolo, J.C. Hanson and C.P. Grey, *J. Am. Chem. Soc*., **123**, 1694-1702, (2001).
22. A. Farrokhina, B. Sakakini and K. C. Waugh, *J. Phys. Chem. B*, **106**, 9567-9575, (2002).
23. E. Kemnitz, G. Hansen, A. Hess and A. J. Kohne., *J. Mol. Catal.* **77**, 193-200, (1992).
24. G. P. Gambaretto, F. Avezzu and E. J. Gola, *J. Appl. Chem. Biotechnol*., **23**, 175-181,(1973).
25. M. Bankhead, G. W. Watson, G. J. Hutchings, J.Scott and D. J. Willock, *Appl. Catal. A*, **200**, 263-274, (2000).
26. Y. Chen and L. Zhang, *J. Catal. Lett*. **12**, 51-62, (1992).
27. A.A.Tsyganenko, P.P. Mardilovich, *J. Chem. Soc., Faraday Trans*. **92**, 4843-4852, (1996).
28. S. Brunet, C. Batiot, J. Barrault and M. Blanchard, *J. Fluorine Chem.* **63**, 227-232, (1993).
29. A. L. Allred, *J. Inorg. Nucl. Chem*., **17**, 215-221, (1961).

30. E. Kemnitz, G. Hansen, A. Hess and A. J. Kohne, *J. Mol. Catal.* **77**, 193-200, (1992).
31. D. R. J. Coulson, *J. Catal*, **142**, 289-302, (1993).